FAILURE ANALYSIS OF A KAPLAN TURBINE RUNNER BLADE

Prof. Dr. Eng. Viorel C. Câmpian
University „Eftimie Murgu" Resita, P-ta Traian Vuia no.1-4, 320085-Resita, Romania
Tel./Fax: 0040 255 219134, E-mail: v.campian@uem.ro
Prof. Dr. Eng. Doina Frunzăverde
University „Eftimie Murgu" Resita, P-ta Traian Vuia no.1-4, 320085-Resita, Romania
Tel.: 0040 255 210 227, Fax: 0040 255 210 230, E-mail: birelex@uem.ro
Prof. Dr. Eng. Dorian Nedelcu
University „Eftimie Murgu" Resita, P-ta Traian Vuia no.1-4, 320085-Resita, Romania
Tel./Fax: 0040 255 219134, E-mail: d.nedelcu@uem.ro
Dr. Eng. Gabriela Mărginean
University of Applied Sciences, Neidenburger Str. 10, D-45877 Gelsenkirchen, Germany
Tel.: 0049 209 9596 353, E-mail: gabriela.marginean@fh-gelsenkirchen.de

ABSTRACT

The paper presents the results of the failure analysis of a Kaplan turbine runner blade from a hydropower station in Romania.

In order to determine the causes that led to the cracks, the authors first carried out metallographic investigations on a sample obtained from the cracked blade. The metallographic investigations included macroscopic and microscopic examinations (light microscopy and scanning electron microscopy) and X-ray diffraction analyzes (XRD). They led to the conclusion that the cracking of the blade was caused by fatigue, initiated by the numerous non metallic inclusions, which were discovered in the vicinity of the blade surface.

The results obtained were confirmed by calculations on the resistance and service life estimations of the blade. The calculations carried out included the following steps: construction of the solid 3D-model of the blade, determination of the blade loads from hydrodynamic conditions, linear static analysis of the blade and service life estimations, calculated for maximal stress values of the concentrators. They led to the conclusion that the cracking of the blade started and developed from the stress concentrator placed between blade and blade flange on leading edge direction.

In order to decrease the maximal stress value, the authors concluded that the hydrodynamic loads on the blade must be obligatory reduced. Therefore, as the operating conditions (discharge, head, speed, power) are not changeable, the stress reduction could be realized only by increasing the number of the runner blades.

KEY WORDS: Hydropower station, Kaplan turbine, fatigue cracking, service life estimations.

1. INTRODUCTION

The analyzed turbine is included in a power plant cascade equipped with low head Kaplan turbines with the same geometrical characteristics (runner with 4 blades-Figure 1), and, although it operates to a higher head compare with the rest of turbines, the solution was promoted from economical reasons.

Figure 1 The runner blade

The technical characteristics of the analyzed turbine are:

- runner diameter D = 5500 mm
- nominal speed n = 115,4 rot/min
- maximal power for net head P_{max} = 35,5 MW
- maximal net head H_{max} = 28,20 m
- calculus net head H_c = 24,0 m
- minimal net head H_{min} = 16,0 m

The calculations of the blade included the following steps:

- the 3D solid modeling of the runner blade, using the Autodesk Inventor software;
- determination of the blade loads from hydrodynamic conditions;
- linear static analyses, for different stress relieve groove geometry and blade number;
- service life estimations, calculated for maximal stress values of the concentrators resulted from COSMOS Design Star software, using Haigh fatigue diagram.

2. METHODOLOGY

2.1. METALLOGRAPHIC INVESTIGATIONS

In order to determine the causes that led to the blade cracking, the sample cut for metallographic investigations, Figure 2, was analysed by light microscopy (LEICA DM 6000M), scanning electron microscopy (Philips XL30 ESEM) and X-ray diffraction (Philips X'Pert).

2.a Positioning of the sample

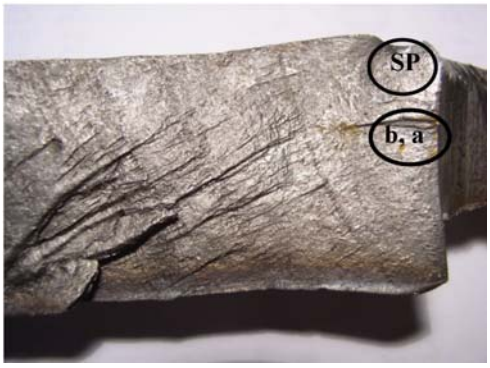

2.b Macrograph of the crack surface, indicating the positions for the SEM-micrographs

Figure 2 Sample cut for metallographic investigations

2.2. THE 3D SOLID MODELLING OF THE RUNNER BLADE

The axial blade turbine is a very complex geometry, which must be generated in a Computer Aided Software (CAD) for the final blade drawing and for finite elements resistance calculus. Autodesk Inventor was chosen as a CAD software. The purpose of the modelling process is to obtain the blade as a solid object and not as a surface, so that it may be used for finite elements resistance calculus. Starting with the plane coordinates of the profiles, the 3D coordinates disposed on cylinders to the radius specified in execution drawings of the runner were calculated, Figure 3.

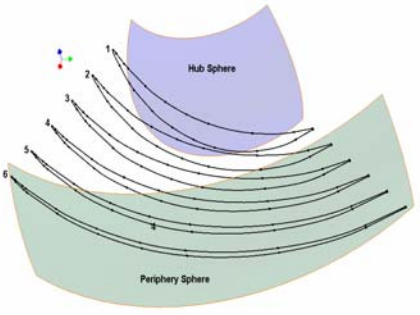

Figure 3 Blade profiles disposed on cylinders

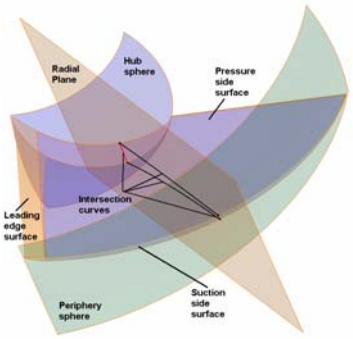

Figure 4 Intersection curves for radial plane

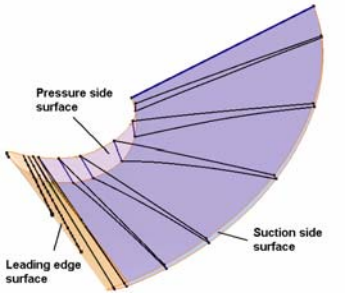

Figure 5 Intersection curves for multiple radial planes

Autodesk Inventor won't generate a valid solid based on a number of closed loops disposed on cylinders or sphere. Therefore the following steps are required:

- generation of the suction side surface, pressure side surface and leading edge surface based on closed loops of the 3D coordinates disposed on cylinders, Figure 4;
- extensions of blade's surfaces: the previous surfaces must be extended to the hub and periphery direction to obtain the surfaces of the complete blade, Figure 4;
- intersections of the blade surfaces with radial planes, disposed at imposed angles, which will generate a number of closed loops disposed on radial planes, Figure 5;
- generation of the solid model of the blade, based on the previous closed loops;
- completion of the 3D solid geometry of the blade with the flange and stress relieve groove with different geometry, Figure 6 and Figure 7.

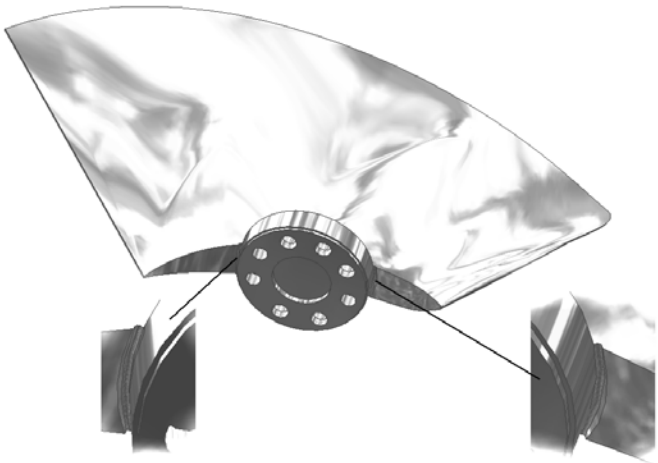

Figure 6 The solid model of the blade with stress relieve groove R8x20

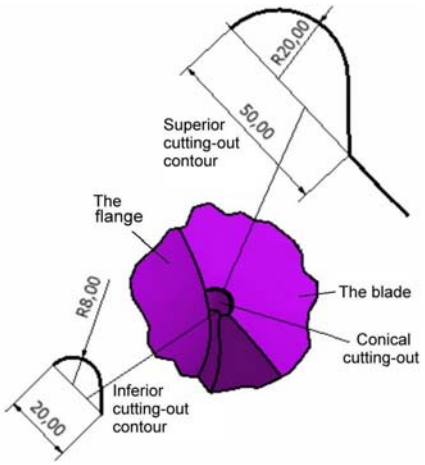

Figure 7 The geometry of the stress relieve groove R20x50

2.3. HYDRODYNAMIC LOADS OF THE BLADE

The hydrodynamic loads applied on the axial runner are presented in Figure 8:

- the gravity load $\vec{G}$;
- the centrifugal force $\vec{F_C}$ for the runner speed 115.4 rot/min;
- the axial thrust $\vec{F_{AH}}$, resulted from the measurements on model;
- the tangential force $\vec{F_T}$,
- $\vec{R}$ is the resultant of the hydraulic force on the blade
- e is the distance to the blade axis.

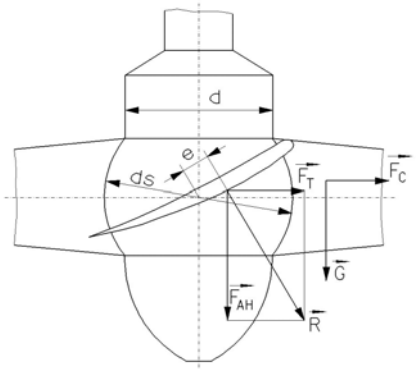

Figure 8 The hydrodynamic loads applied to the runner

3. EXPERIMENTAL AND NUMERICAL RESULTS

3.1. METALLOGRAPHIC INVESTIGATIONS

Examining the crack surface shown in Figure 2.b, one can observe the specific appearance of fatigue cracking [1]. The surface is smoothened, resulting from the relative friction of the two pieces of the cracked blade one upon the other, during the alternated loads. The positions of the fan-shaped striations indicate that the cracking started from the region marked with "SP" (starting point) in Figure 2.b. The SEM-micrographs of the regions "a" and "b" positioned in Figure 2.b are presented in Figure 9.

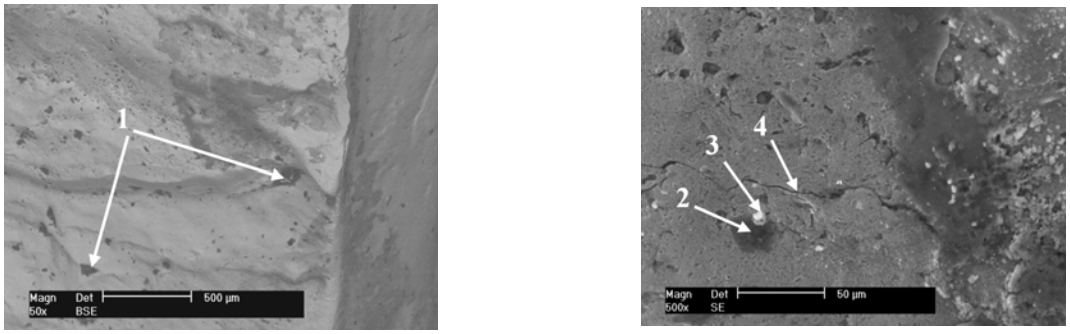

9.a BSE, 50x 9.b SE, 500x

Figure 9 SEM-micrographs of the crack surface

The images shown in Figure 9 indicate a high content of non-metallic inclusions in the blade material (marked with 1 in Figure 9.a). During the crack propagation, the operating water determined the corrosion of the base material surrounding these inclusions. As a consequence, the non-metallic inclusions released from the surface, leaving craters behind (position 2 in Figure 9.b), which were filled in with corrosion products (positioned by 3 in Figure 9.b)

In the surface of the investigated sample numerous secondary cracks (as marked by 4 in Figure 9.b) were observed, which are specific for fatigue cracking [2], [3].

After SEM-examination, the crack surface was grinded, polished and examined again with the scanning electron microscope. Globular non-metallic inclusions could be observed also in this surface, as well as the surrounding corrosion attack of the metallic material (Figure 10.a). The XRD-analyze led to the conclusion that these inclusions are silicates and oxides (Figure 10.b).

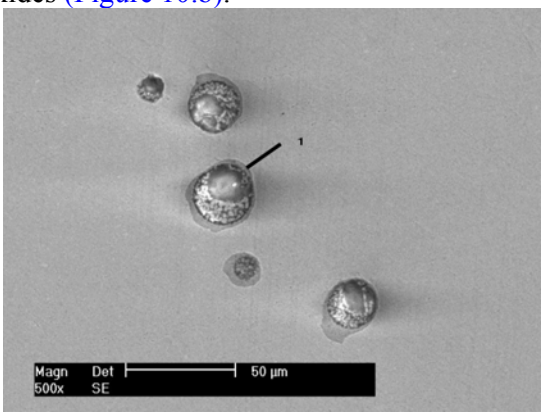

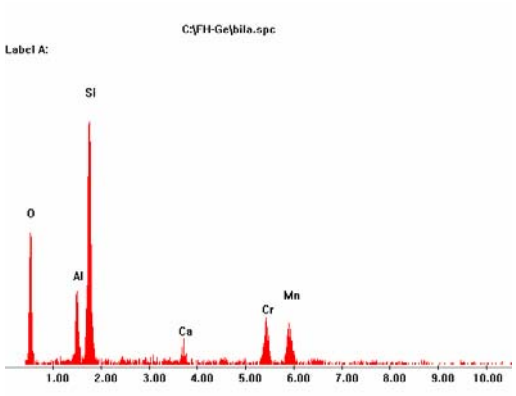

10.a SEM-micrograph 10.b XRD-capture of the inclusions

Figure 10 Non-metallic inclusions in the vicinity of the crack surface

After etching of the metallographic sample one could visualize the microstructure of the blade material, Figure 11, consisting of martensite and soft ferrite islands, with grid-like distribution. Both, the relative high percentage of oriented ferrite and the important content of non-metallic inclusions are not usual for this kind of applications.

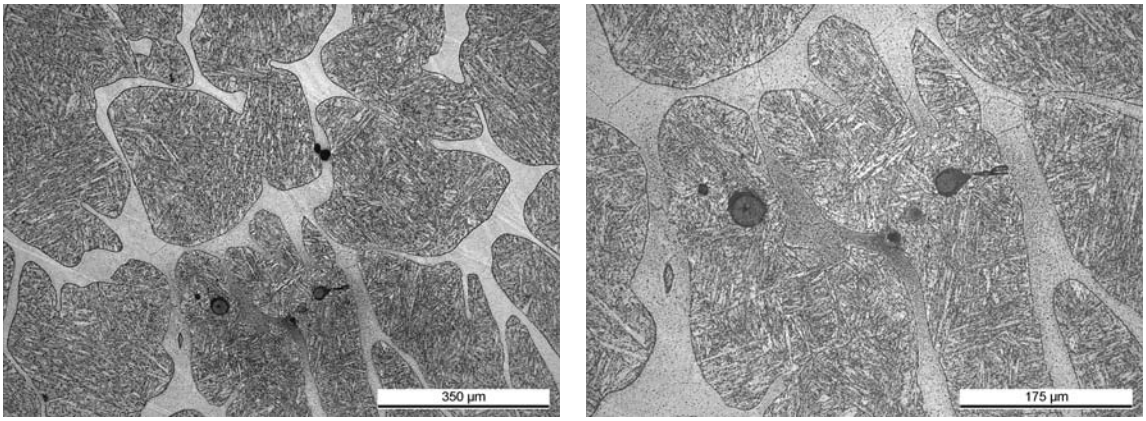

Figure 11 Structure of the blade material

The metallographic investigations finally led to the conclusion that the cracking of the blade was caused by fatigue. The crack propagation occurred gradually, through development of the principal cracking front. Because of the high content of non-metallic inclusions and the inhomogeneous structure of the blade material, additionally numerous secondary cracks developed inside the material.

After the failure was initiated by fatigue, the crack surfaces were exposed to chemical corrosion processes. This phenomenon was accentuated and accelerated by the presence of the high content of non metallic inclusions.

3.2 NUMERICAL DATA

Table 1 presents the operation points considered for resistance calculus, which correspond to the following power values: 35.5 MW, 30 MW, 25 MW, 20 MW and 15 MW at different head values. The axial thrust and tangential forces were calculated for 4 and 6 runner blade. The placement of the operating points in the prototype hill chart is shown in Figure 12.

Table 1

Operation point	UM	Blade number	**1**	**2**	**3**	**4**	**5**	**6**	**7**
P	MW	-	35.5	35.5	30	30	30	30	25
H	m	-	28.2	24	28.2	24	23	22	28.2
Q	m^3/s	-	143.59	168.00	121.90	140.62	146.25	153.12	102.56
F_{AH} / blade	N	4	878642	762300	878642	771375	747931	715413	863713
F_{AH} / blade	N	6	585761	508200	585761	514250	498621	476942	575809
F_T / blade	N	4	381508	381508	322401	322401	322401	322401	268667
F_T /blade	N	6	254338	254338	214934	214934	214934	214934	179112
Operation point	UM	Blade number	**8**	**9**	**10**	**11**	**12**	**13**	**14**
P	MW	-	25	25	25	25	20	20	20
H	m	-	24	23	22	21	27.5	24	23
Q	m^3/s	-	118.03	122.48	127.24	132.98	84.74	95.65	99.43
F_{AH} / blade	N	4	780450	761846	732050	698775	873469	794970	765325
F_{AH} / blade	N	6	520300	507898	488033	465850	582313	529980	510217
F_T / blade	N	4	268667	268667	268667	268667	214934	214934	214934
F_T / blade	N	6	179112	179112	179112	179112	143289	143289	143289
Operation point	UM	Blade number	**15**	**16**	**17**	**18**	**19**		
P	MW	-	20	20	15	15	15		
H	m	-	22	21	23	22	21		
Q	m^3/s	-	103.40	176.81	75.84	79.08	82.54		
F_{AH} / blade	N	4	740369	674953	765325	743696	722597		
F_{AH} / blade	N	6	493579	449969	510217	495798	481731		
F_T / blade	N	4	214934	214934	161200	161200	161200		
F_T / blade	N	6	143289	143289	107467	107467	107467		

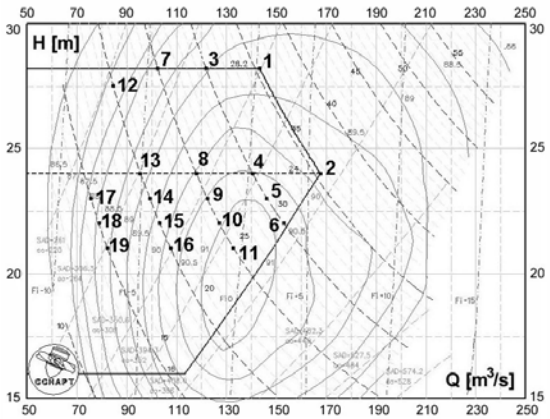

Figure 12 The placement of the operating points in the prototype hill chart

3.3 LINEAR STATIC ANALYSIS OF THE BLADE

The study was made with the Cosmos Design Star software, which offers a wide range of advanced type analyses: linear static analysis and nonlinear analysis, frequency analysis, linearized buckling analysis and thermal analysis.

Figure 13 show the loads and restrictions applied to the blade:

- *Fixed* type constraints applied to the flange holes, which impose 0 value for the translations and rotations of the selected entities;
- axial thrust F_{AH};
- tangential force F_T;
- centrifugal force F_c;
- blade gravity G.

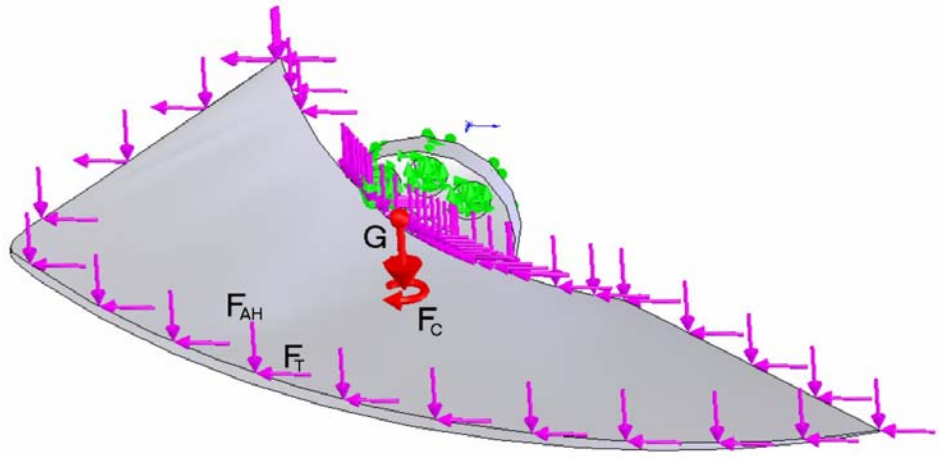

Figure 13 Loads and restrictions applied to the blade

Because the blade cannot be generated as a surface with constant thickness, for finite element analyse, only solid mesh (parabolic tetrahedral solid elements) can be used. The mesh is shown in Figure 14. For original stress relieve groove R8x20 a local fine mesh was used, Figure 15. The results are presented numerically in Table 2, and graphically in Figure 16 and Figure 17, only for operating point no. 1.

Figure 14 The blade mesh

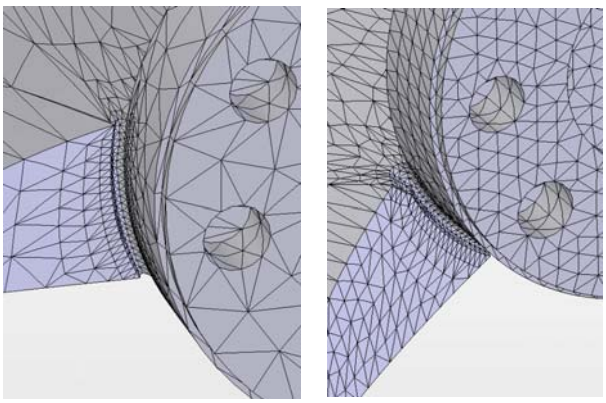

Figure 15 The blade mesh in the stress relieve groove area

Numerical results for stress relieve groove R8x20 (4 blades) Table 2

Operation point	1	2	3	4	7	8	12	13	17
Head H [m]	28.2	24	28.2	24	28.2	24	27.5	24	23
Power P [MW]	35.5	35.5	30	30	25	25	20	20	15
VonMises Stress	474.7	434	467.7	447.5	475.4	444.6	472.7	443.6	426.4
Maximum Displacement	20.47	17.97	20.27	17.55	19.32	17.57	19.35	17.7	16.91

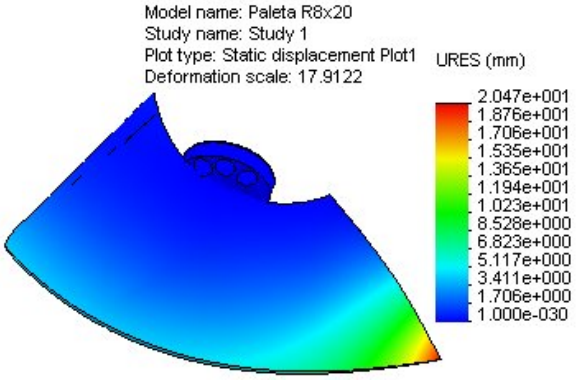

Figure 16 The resultant displacement plot

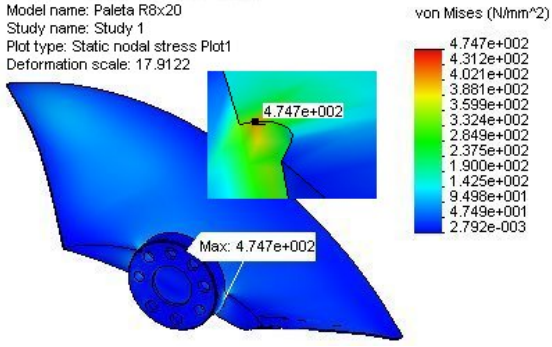

Figure 17 The Von Mises stress plot

To reduce the maximal stress values, the geometry of the stress relieve groove was modified from R8x20 to R20x50, Figure 7. The results are numerically shown in Table 3.

Numerical results for stress relieve groove R20x50 (4 blades) Table 3

Operation point	1	2	3	4	7	8	12	13	17
Head H [m]	28.2	24	28.2	24	28.2	24	27.5	24	23
Power P [MW]	35.5	35.5	30	30	25	25	20	20	15
VonMises Stress	426.3	388.8	421.0	386.4	411.4	384.6	409.8	384.5	370.1
Maximum Displacement	20.47	17.97	20.28	17.98	19.78	17.99	19.82	18.13	17.32

Table 3 presents a reducing of the Von Mises stress values for a power range of 30…15 MW, but not enough to promote the solution. In these circumstances, the blade loads can be reduced by blade number increasing. Table 4 shows the numerical results for stress relieve groove R8x20 with 6 blades. A significant decreasing of the stress and displacements values can be observed, comparing with the previous solutions.

Numerical results for stress relieve groove R8x20 (6 blades) Table 4

Operation Point	1	2	3	4	7	8	12	13	17
Head H [m]	28.2	24	28.2	24	28.2	24	27.5	24	23
Power P [MW]	35.5	35.5	30	30	25	25	20	20	15
VonMises Stress	357.3	330.0	352.7	339.9	358.4	337.9	356.6	337.3	325.8
Maximum Displacement	13.76	12.09	13.63	11.82	12.99	11.83	13.01	11.92	11.39

3.4 SERVICE LIFE ESTIMATIONS

For service life estimations a standard procedure for hydraulic turbine is used, for the operating points with maximal stress values. The amplitude oscillation for Kaplan blade turbine is experimentally obtained and is around 20 MPa. The yield strength value of the blade material is $R_{P0,2\ min}$=550 MPa. The calculated values of the stress for stress relieve groove R8x20 and R20x50 and 4 blades were introduced in Haigh diagram, Figure 18 [4].

From Haigh diagram results that, for stress relieve groove R8x20, the blade cracks should be obtained between $10^9 \div 10^{10}$ of the fatigue cycles. To reduce the stress concentrator values, a number of different stress relieve groove geometry were studied. The optimal solution was obtained for stress relieve groove R20x50, where the stress values were reduced in the range between 45...60 MPa (see Table 3 and Figure 18), but not enough to promote as a final solution.

The results from Figure 18 are ideally, because the fatigue curves are obtained in laboratory for samples with controlled chemical composition and homogeneity, with no fissures and surfaces or deeply defects. For these reasons, in service life estimations and fatigue calculus is recommended that the stress concentrator values will not be higher than half of yield strength value of the material, in our case 275 MPa.

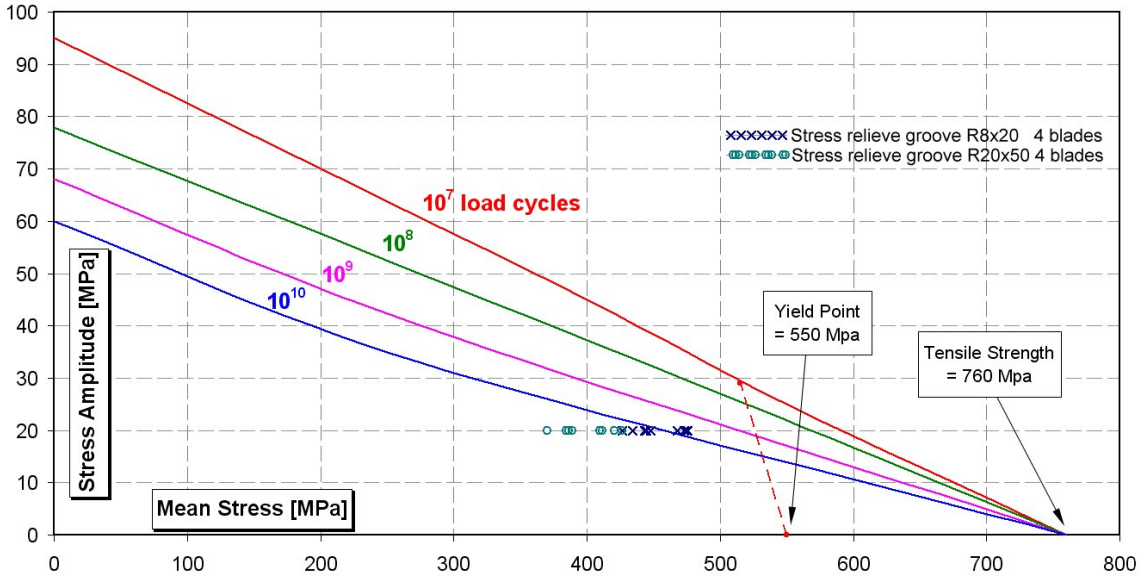

Figure 18 The Haigh diagram

4. CONCLUSIONS

The calculations carried out led to the conclusion that the cracking of the blade started and developed from the stress concentrator placed between blade and blade flange on leading edge direction.

A few stress relieve groove geometry were analysed, but did not generate a decreasing of the stress concentrators in admissible limits (smaller than half of yield strength value of the material). This effect cannot be obtained only by modifying the stress relieve groove geometry.

In order to decrease the maximal stress value it is necessary to reduce the hydrodynamic loads on the blade. For existing operating conditions (discharge, head, speed, power), the stress decreasing is possible only by increasing the number of the runner blades.

To accentuate this conclusion, for the same blade geometry, a blade with stress relieve groove R8x20 was calculated, but for 6 blades. The results show a significant decreasing of the stress concentrators values (about 100 MPa) which, associated with an optimal stress relieve groove geometry, can lead to a stress reducing in admissible limits. These calculus are theoretically, because they are made for a runner with 6 blades and the same geometry of the blade. But, a new runner, with 5 or 6 blades, will require a new blade geometry (new profiles, a blade with a smaller extensions), and, therefore, the loads will be modified.

ACKNOWLEDGEMENT

The work have been supported by the MATNANTECH program, project CEEX-M1-C2-1185, contract no. 64/2006, acronym *iSMART-flow*. Numerical computations and experimental investigations have been performed at ExpertLAB from the Research Centre in Hydraulics, Automation and Heat Transfer, „Eftimie Murgu" University of Reşiţa (www.cchapt.ro) and at the Laboratory for Material Science and Material Testing, University of Applied Sciences, Gelsenkirchen.

REFERENCES

[1] LANGE G., 2001, *Systematische Beurteilung technischer Schadensfälle, 5.Auflage,* Wiley - VCH Verlag, D-69469 Weinheim, Germany, pg. 103-147.
[2] LANGE G., 2001, *Systematische Beurteilung technischer Schadensfälle, 5.Auflage,* Wiley - VCH Verlag, D-69469 Weinheim, Germany, pg. 163.
[3] SCHMIDT P.F., 1994, *Praxis der Rasterelektronenmikroskopie und Mikrobereichsanalyse,* Expert Verlag, Renningen - Malmsheim, Germany, pg. 103-147.
[4] HELMUT KECK, June 29, 2004, *Stakeholders perspectives on the challenges or threats and on "A European research network as one instrument to effective rehabilitation and utilization of European hydropower Infrastructure",* ELFORSK WORKSHOP, Stockholm, Sweden.